nature communications

Article

https://doi.org/10.1038/s41467-025-61969-7

A unimolecule nanopesticide delivery system applied in field scale for enhanced pest control

Received: 20 May 2024

Accepted: 7 July 2025

Published online: 24 July 2025

Check for updates

Xingye Li[1], Xinyue Wang[1], Changjiao Sun[1], Anqi Wang[1], Changcheng An[1], Ningjun Li[1], Yue Shen[1], Jiachong Hu[1], Huihui Liu[1], Jing Xie[1], Dan Luo[2] & Yan Wang[1]

Nanopesticides provide immense potential in reducing pesticide use and promoting sustainable agriculture for their enhanced pesticidal efficacy. Nano-enabled delivery systems can enhance pesticide penetration into both insects and leaves through their unique nanoproperties, in particular their small size. However, it remains a great challenge to achieve unimolecular formulations in water-based processes in order to take full advantages of nanoproperties. Here, using ionic liquid, we fabricate unimolecular nanopesticides (about 3 nm in average diameter) in a water-based process, termed unimolecule-nanopesticide delivery system. Guided by the density functional theory calculations, we successfully convert various traditional pesticides into the unimolecule-nanopesticide system, significantly enhancing cellular uptake, insect-dermis translocation, and leaf-cuticle penetration of pesticides. Furthermore, we improved field efficacy against multiple pests using the unimolecule-nanopesticide system. Importantly, the unimolecule-nanopesticide system utilizes only industry-grade raw materials that are Generally Recognized as Safe by the US Food and Drug Administration. We believe our unimolecule-nanopesticide system represents a water-based and facile-manufactured platform for other conventional pesticides to achieve high-efficiency field-scale plant protection.

Ineffective control of plant pests and diseases accounts for ~20–40% of global crop losses annually, leading to an economic loss of around US $270 billion per year[1]. Plant pests and pathogens also consequently threaten global food security, making pesticides an irreplaceable component of modern agriculture[2–4]. The development of highly efficient pesticide delivery systems is a crucial strategy for achieving better plant protection[5–8]. Recent advancements in nano-enabled delivery system provide immense potential in reducing economic loss and promoting sustainable agriculture[9–13]. Over the past decade, a series of nanopesticides (NPs) have been developed with a reported increase in pesticidal efficacy and decrease in toxicity compared to their non-nanoscale counterparts[14]. Nanomaterials, with their small size, large surface area, tunable structures, and modifiable surface chemistry, offer significant advantages in achieving smart release and targeted delivery of pesticides[15]. Multiple factors interactively influence the efficacy and safety of nanopesticides in the field, including particle size, physicochemical properties, formulation types, release properties, and application performance[14].

While great efforts have been exerted to make pesticides environmentally friendly by using green solvents such as ethanol and

[1]Institute of Environment and Sustainable Development in Agriculture, Chinese Academy of Agricultural Sciences, Beijing, PR China. [2]Department of Biological and Environmental Engineering, Kavli Institute at Cornell for Nanoscale Science, Cornell University, Ithaca, NY, USA.
e-mail: wangyan03@caas.cn

water[16–21]. Widely used water-insoluble commercial insecticides, such as emamectin benzoate (EMB), spinosad (SPS), abamectin, lambda-cyhalothrin, lufenuron, etc., are typically processed in harmful organic solvents for better penetration into the insect dermis through contact and/or leaf cuticle through foliar treatment[22–25]. Typical organic solvents include toluene, xylene, high boiling aromatic solvent oil (such as S-200, naphtha S-100). It is more desirable to replace organic solvents with water-based processes to improve environmental friendliness[26,27].

An attractive solution for the water-based system has been demonstrated in herbicidal ionic liquids (HILs), which have brought revolutionary changes to the field of agrochemicals with their superior environmental compatibility and efficacy[28–35]. By reducing the reliance on harmful solvents and surfactants, they have not only improved weed control but also mitigated environmental impacts[36–41]. However, few reports describe an IL-based NPs system for transdermal and trans-leaf cuticle pest control due to the challenging barriers of insect cuticles and leaf surfaces. We expect that IL can achieve tuned nanopesticides in a fully water-based process and significantly enhance insecticide efficacy.

It has been reported that the pesticidal efficacy will increase even more with the further size reduction[19,42–44]. The importance of NP sizes lies in the fact that the smaller the NPs, the better their penetration of insects and leaves[19,42–44]. However, achieving NP sizes down to the ultimate smaller size (the unimolecular size) in a water-based process remains a great challenge. Although current methods, such as microemulsion and nanoemulsion, have achieved smaller sizes of NPs[45], they usually require organic solvents and cannot achieve unimolecular level. Thus, it is important to develop a unimolecular NPs manufactured platform with an environmentally friendly water-based process to enhance pest control.

In this study, we have developed a facile-synthesized and highly efficient unimolecule-nanopesticide (UNI) delivery system. Our UNI system is an almost mono-dispersed system consisting of NPs in a 3 nm-sized unimolecular structure with IL as a high-efficiency carrier (Fig. 1a and Supplementary Fig. 1a). We characterized our UNI system with various approaches, including density functional theory (DFT) calculation and molecular dynamics (MD) simulation, penetration measurement, field-scale experiment, and safety assessment (Fig. 1 and Supplementary Fig. 1b). Our UNI system demonstrates enhanced pesticide bioactivity, field-scale efficacy against multiple pests, safety for plants and non-target organisms, and reduced pesticide residues on crops (Fig. 1b-e). This study systematically demonstrates the formation process of the unimolecule-nanopesticide delivery system to improve the transdermal and foliar penetration of pesticides while enhancing their efficacy and safety.

Results

Construction, characterization and self-assembly mechanism of a unimolecule-nanopesticide (UNI) delivery system

The basic components of our UNI system consist of only IL and water before the addition of pesticide payloads. Besides water, we chose commercially available, low-cost industry-grade choline chloride and sodium dodecyl sulfate as the raw materials for synthesizing IL through ionic interactions rather than covalent bonds (Supplementary Fig. 1c). We used eighteen different ILs and selected choline dodecyl sulfate (CDS) due to its ability to form the smallest particles among the tested ILs in water (Supplementary Fig. 2). Moreover, CDS exhibited the best potential for dermal penetration, according to the findings of Samir Mitragotri's group; they reported that ILs with fewer cross-peaks indicated weak ion interactions and often exhibiting enhanced transdermal delivery[46]. Indeed, we observed only nine cross-peaks for dodecyl sulfate-based ILs through nuclear Overhauser effect spectroscopy (NOESY) analysis; this number was lower than that of most fatty acid-based ILs, which are common penetration enhancers. (Supplementary Fig. 3).

Most pesticides have low solubility in water; for those pesticides that use water-based formulations, such as suspension concentrate (SC), their sizes are typically large, ranging from 100 nm to micrometers. For this study, we chose emamectin benzoate (EMB) as our model pesticide for the payload. EMB is one of the most widely used pesticides, known for its high efficiency and broad-spectrum properties. More importantly, EMB has very limited water solubility, which has been notably difficult to achieve unimolecular size in organic-solvent-free processes.

We utilized our UNI system (CDS + water) to reduce EMB to the unimolecular size, resulting in a stable water-based formulation. In more detail, we discovered that EMB and CDS were able to self-assembled in water; the assembled sizes were controlled by the mass ratio of EMB to CDS. At a 1:5 ratio, the UNI-EMB particle sizes were 2.9 ± 0.4 nm based on TEM (Fig. 2a, b). Notice that the TEM size of the UNI system alone, without EMB, was 1.7 ± 0.3 nm (Supplementary Fig. 4). Considering that the size of a single EMB molecule, as calculated by DFT, is 1.2–2.3 nm (Supplementary Fig. 4d), this suggests that our UNI-EMB has reached the unimolecular pesticide state. This conclusion was further verified by the hydrodynamic radius determination through dynamic light scattering (DLS) analysis (Fig. 2b and Supplementary Fig. 4c). As a control, the system with an EMB/CDS ratio of 1:1 resulted in much larger complexes: 111.1 ± 16.4 nm and 92.6 ± 0.2 nm by TEM and DLS, respectively (Fig. 2c, d). We further confirmed the unimolecular size of about 3 nm through small-angle X-ray scattering (SAXS) (Fig. 2e, Supplementary Table 1)[47]. Moreover, we observed a unimolecular EMB carried by 12-15 ionic liquid clusters through matrix-assisted laser desorption/ionization time-of-flight mass spectrometry (MALDI-TOF-MS), as shown in Supplementary Fig. 5.

To further characterize the UNI-EMB system, we systematically examined the potential interactions between EMB and CDS using proton nuclear magnetic resonance (^{1}H NMR) analysis in D_2O (Supplementary Fig. 6). The ^{1}H NMR spectra of UNI-EMB exhibited no significantly broadened peaks, suggesting a good dispersion state; in contrast, IL-EMB$_{111nm}$ exhibited four broadened peaks. The structures and spatial interactions of EMB and CDS were further characterized using 2D NOESY analysis (Fig. 2f, g and Supplementary Fig. 7)[46]. The NOESY spectrum of UNI-EMB demonstrated at least seven cross-peaks between the EMB cation (EM^+) and CDS anion (DS^-), indicating their strong spatial interactions (Fig. 2f). Conversely, the NOESY spectrum of IL-EMB$_{111nm}$ exhibited no intermolecular nuclear Overhauser effects (NOEs), due to the extensive aggregation of suspension particles in the system (Fig. 2g). As shown in Fig. 2f and Supplementary Fig. 7, a cross-peak is observed between the proton on the positively charged center N^+-H of EM^+ and the proton on the negatively charged center $^-$O-S-O-CH_2 of DS^-, indicating a strong electrostatic interaction between EM^+ and DS^-. Moreover, several cross-peaks between the hydrophobic tail of EM^+ and the hydrophobic carbon chain of DS^- confirm the presence of intermolecular hydrophobic interactions. Therefore, our NMR analyses strongly suggest that our UNI system has strong spatial interactions between pesticide and IL, exhibiting unimolecular dispersion.

To gain a qualitative understanding of the configurations leading to the unimolecular state, Independent Gradient Model (IGM) map and Independent Gradient Model based on Hirshfeld Partition (IGMH) analysis were performed to investigate noncovalent interactions in real space based on electron density (Fig. 2h)[48–55]. The IGM map revealed the presence of strong electrostatic interactions between the EM^+ and DS^- in the blue transition area (Fig. 2h, red circle), and meanwhile, strong van der Waals interactions in the green transition area (Fig. 2h, red dashed circle). Additionally, the IGMH map revealed the presence of hydrogen bonds between EMB and CDS, with a total hydrogen bond energy being −23.00 kcal/mol (Supplementary Fig. 8). By combining the results of NOESY experiments and DFT (IGM plus IGMH) calculations and found that there is a strong interaction between the EM^+ and DS^-, suggesting the formation of UNI.

https://doi.org/10.1038/s41467-025-61969-7

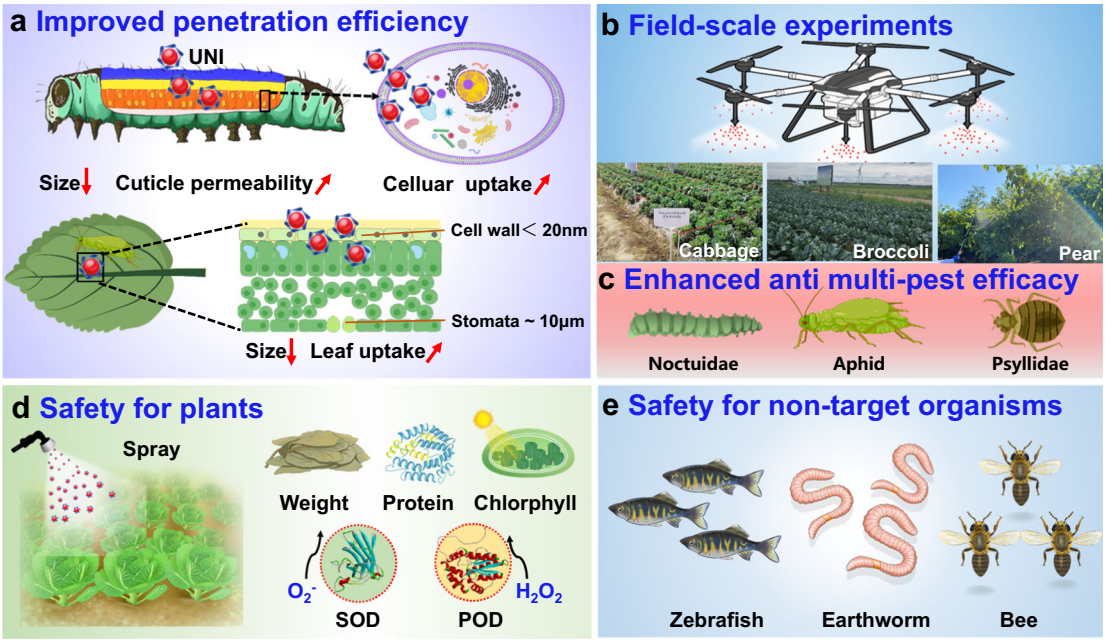

Fig. 1 | Schematic representation of a unimolecule-nanopesticide (UNI) delivery system. a The UNI demonstrates exceptional cellular uptake capability and enhanced permeability across both insect dermal and leaf cuticle layer, thereby enhancing pesticide bioactivity. **b** The UNI system for field-scale plant protection. **c** The UNI shows enhanced field control efficacy against multiple pests, including *Spodoptera exigua*, *Brevicoryne brassicae*, and *Psylla chinensis*. **d** Safety for plants. **e** Safety for non-target organisms.

To gain a better understanding of the UNI formation mechanism, we selected NP10, an additive commonly used in commercial formulations. We performed molecular dynamics (MD) simulations to compare the UNI-EMB and NP10-EMB systems (Fig. 2i, Supplementary Fig. 9)[53,54,56–58]. According to the MD results, the interaction force between EMB and CDS is −9450 kJ/mol, which is greater than −4471 kJ/mol for the interaction between EMB and NP10, where the Coulombic force $E_{Coul(UNI\text{-}EMB)}$ = −7285 kcal/mol is significantly larger than $E_{Coul(NP10\text{-}EMB)}$ = −2087 kcal/mol. This suggests that electrostatic interactions play a crucial role in the formation of UNI. Additionally, the simulation results show that EMBs exhibits nearly unimolecular dispersion in the UNI system, while the other ones in the NP10-EMB system showcase a fully aggregate state. In summary, our MD results indicate that the strong interaction forces between CDS and EMB, including electrostatic interactions, van der Waals forces, and hydrogen bonds, are the main reasons for the formation of UNI.

In conclusion, combined with the results of our experiments, calculations, and molecular simulation, we propose the possible mechanisms for the formulation of UNI: (1) electrostatic interactions; (2) hydrophobic interactions; (3) hydrogen bonding.

UNI-EMB penetration ability and bioactivities

To investigate the ability of the UNI system to penetrate insect dermis and cells (Fig. 3), a fluorescently labeled derivative (emamectin 1-naphthaleneacetate, E*) was synthesized (Supplementary Fig. 10). We employed *Spodoptera exigua* (Hübner) third instar larvae for ex vivo transdermal penetration using the dipping method, a major polyphagous pest with global distribution (Fig. 3a)[59]. Our findings demonstrate that the majority of EMB delivered by UNI was distributed within the endodermis, while IL-EMB_{111nm} exhibited lower penetration efficiency (Fig. 3b). The results revealed that the endodermis fluorescence intensity of UNI-EMB was 4.1-fold higher than that of IL-EMB_{111nm}, 1.6-fold higher than the commercial microemulsion (ME), and 2.6-fold higher than the commercial soluble granule (SG) group (Fig. 3d and Supplementary Fig. 11). The particle size is a primary determinant of insect body penetration.

At the cellular level, we examined cellular delivery/association in High Five cells using confocal laser scanning microscopy (CLSM) and flow cytometry. Our results demonstrate that fluorescence intensities of the UNI-EMB were 1.7-fold (via CLSM) and 2.1-fold (via flow cytometry) stronger compared to that of IL-EMB_{111nm} (Fig. 3c, e, Supplementary Fig. 12). These cellular data support the notion that the smaller the size, the higher the penetrability.

The bioactivities of UNI-EMB were systematically evaluated using third instar larvae of *Spodoptera exigua* (Hübner) to investigate its potential for controlling pests in agricultural applications. Our results demonstrate that the reduction in size significantly enhanced its efficacy, leading to an increased mortality rate of *S. exigua* (Fig. 3g and Supplementary Fig. 13). Specifically, at 24 h post-treatment, the mortality rates were at least 40% higher in insects treated with UNI-EMB at all tested concentrations, compared to those treated with IL-EMB_{111nm}. At the concentration of 100 mg·L^{-1}, to reach a 50% mortality rate, UNI-EMB needed only 4 h compared to IL-EMB_{111nm} which took 24 h. Furthermore, we compared our UNI system with ME and SG in terms of bioactivity (Fig. 3h, i, Supplementary Table 2). The toxicity (based on LC_{50} value) of UNI-EMB against *S. exigua* on contact was 2.8 and 5.2 times higher than that of the commercially formulated ME and SG, respectively.

To further investigate ionic liquids as an important green component in our UNI systems, we also compared them with a number of commercial surfactants in terms of their performance in preparing nano-pesticides. As shown in Supplementary Fig. 14a, the particle size of the formulations prepared using a number of commercial surfactants was hard to achieve unimolecular sizes; in contrast, their sizes were all above 400 nm. Meanwhile, they exhibited larger surface contact angles on leaves (Supplementary Fig. 14b). We successfully prepared a unimolecular system that commercial surfactants could not achieve. Moreover, the UNI system prepared using ionic liquids exhibited more efficient cellular uptake and increased mortality rate of the target pest (Supplementary Fig. 13c, d).

For foliar application against sap-sucking pests, efficient uptake of pesticides by leaves is crucial[60]. The distribution of UNI-EMB, IL-EMB_{111nm}, commercial ME, and SG on the surfaces of pear leaves was

https://doi.org/10.1038/s41467-025-61969-7

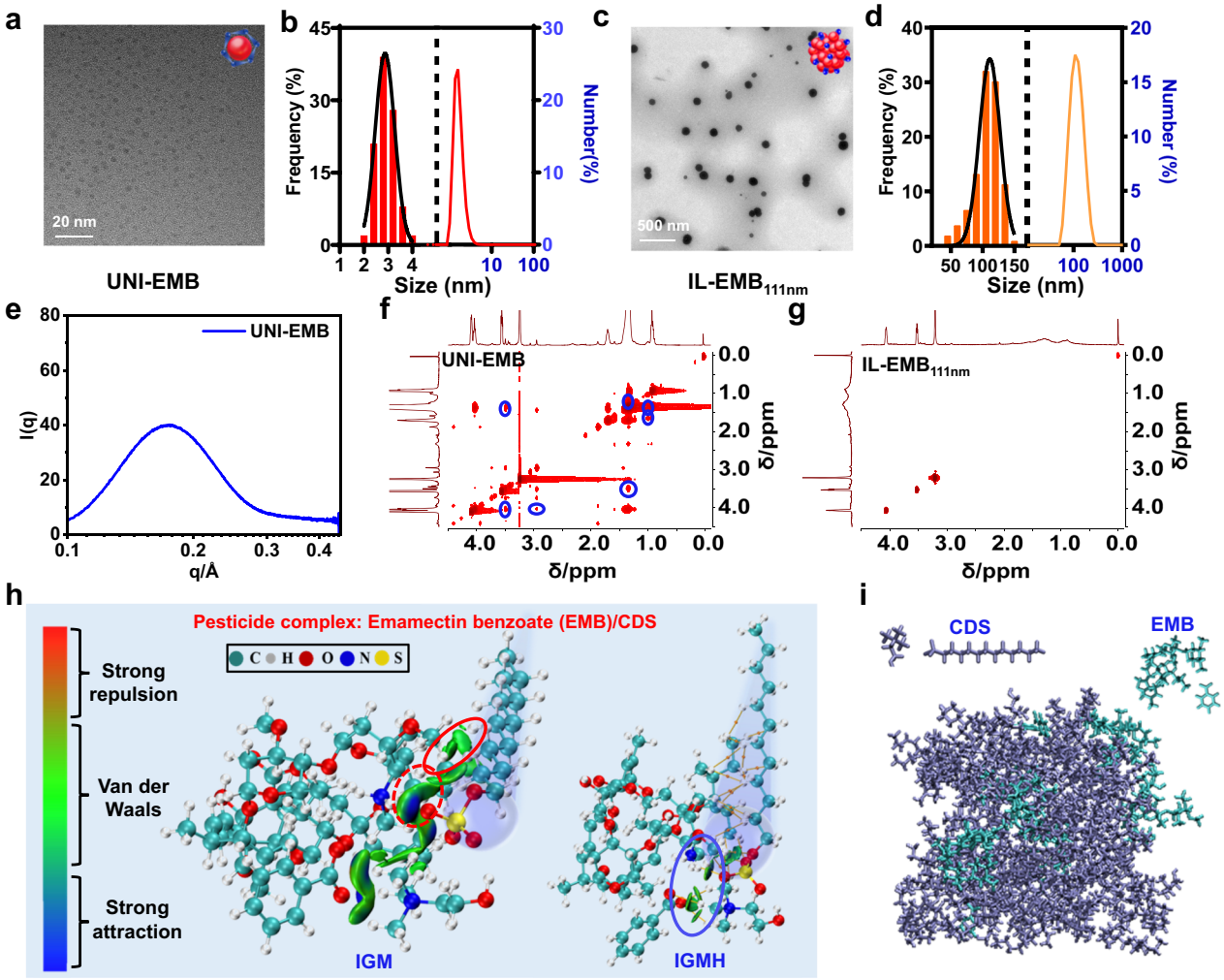

Fig. 2 | Characterization and self-assembly mechanism of the UNI delivery system. a High resolution transmission electron microscopy (HRTEM) image of UNI-emamectin benzoate (EMB). The experiments were independently repeated three times with similar results. **b** left, distribution of particle sizes (diameter) based on the UNI-EMB HRTEM image; right, UNI-EMB's particle size (diameter) distribution using a laser particle size analyzer. **c** High resolution transmission electron microscopy (HRTEM) image of IL-EMB$_{111nm}$. The experiments were independently repeated three times with similar results. **d** Left, distribution of particle sizes (diameter) based on the IL-EMB$_{111nm}$ HRTEM image; right, IL-EMB$_{111nm}$'s particle size (diameter) distribution using a laser particle size analyzer. **e** Small-angle X-ray scattering (SAXS) data of UNI-EMB (diameter size). Nuclear Overhauser effect spectroscopy (NOESY) spectra of IL-EMB$_{111nm}$ (**f**) and UNI-EMB (**g**). The blue circles show cross-peaks between EMB and CDS. **h** Independent gradient model (IGM) diagram of the EMB/CDS (left) and independent gradient model based on Hirshfeld partition (IGMH) diagram (right). The red/dashed/blue circle shows different noncovalent interactions. **i** Molecular dynamics (MD) simulations of UNI-EMB.

investigated using CLSM with E* as a highly effective fluorescent marker[43]. Sudan IV was used as a fluorescence marker for the cuticle, and merged images were provided. Due to the advantageous size effect of unimolecular dispersion, UNI-EMB exhibited the most extensive coverage across the leaf surface compared to the larger size IL-EMB$_{111nm}$ (Fig. 4a, b). Z-stack profiles (Fig. 4c and Supplementary Fig. 15a) and quantitative analysis (Supplementary Fig. 15b) revealed that the intracellular fluorescence intensity of UNI-EMB was significantly higher than those of IL-EMB, ME, and SG. These profiles showed that the fluorescence depth within pear leaves after treatments with UNI-EMB, IL-EMB$_{111nm}$, commercial ME, and SG was 8 μm, 2 μm, 4 μm, and 4 μm, respectively. These findings suggest that the UNI treatment enhances pesticide uptake in leaves and potentially exhibits superior efficacy against sap-sucking pests due to its small size and unimolecular structure.

Field insecticidal efficacy of the UNI-EMB

To explore the multi-pesticidal activities in the real world (the field scale, Fig. 5), we evaluated field efficacy with two different types of larvae: a chewing pest, *S. exigua* (Fig. 5a); and two sap-sucking pests, *Brevicoryne brassicae* (Fig. 5c) and *Psylla chinensis* (Fig. 5e)[61]. We selected commercial pesticides ME and SG as our field comparison controls. At the same concentration across the three formulations, our UNI-EMB achieved the highest field pesticidal efficacy against all pests throughout all test durations, surpassing all the commercial controls (indicated by solid red bars in Fig. 5b, d, f). In addition, even when we reduced the concentration of UNI-EMB, we observed the same multi-pesticidal efficacy as the commercial controls (Hatched red bars in Fig. 5b, d, f).

The effectiveness of pesticides applied in the field is influenced by several factors, and foliar spray is the first step of field application. Minimizing the loss of pesticide droplets is key to improving the efficacy[5]. Compared with commercial SG, UNI can quickly anchor onto the leaf with fewer broken droplets and shows a larger spreading surface area during droplet impact (Supplementary Fig. 16a). Meanwhile, UNI achieved good foliar surface spreading with a smaller contact angle of 52 ± 2° on superhydrophobic leaves compared to SG (82 ± 3°) (Supplementary Fig. 16b). Additionally, the release of pesticides after spreading on crop leaves, as well as the subsequent diffusion behavior of pesticides on targets, can further affect the efficacy of

https://doi.org/10.1038/s41467-025-61969-7

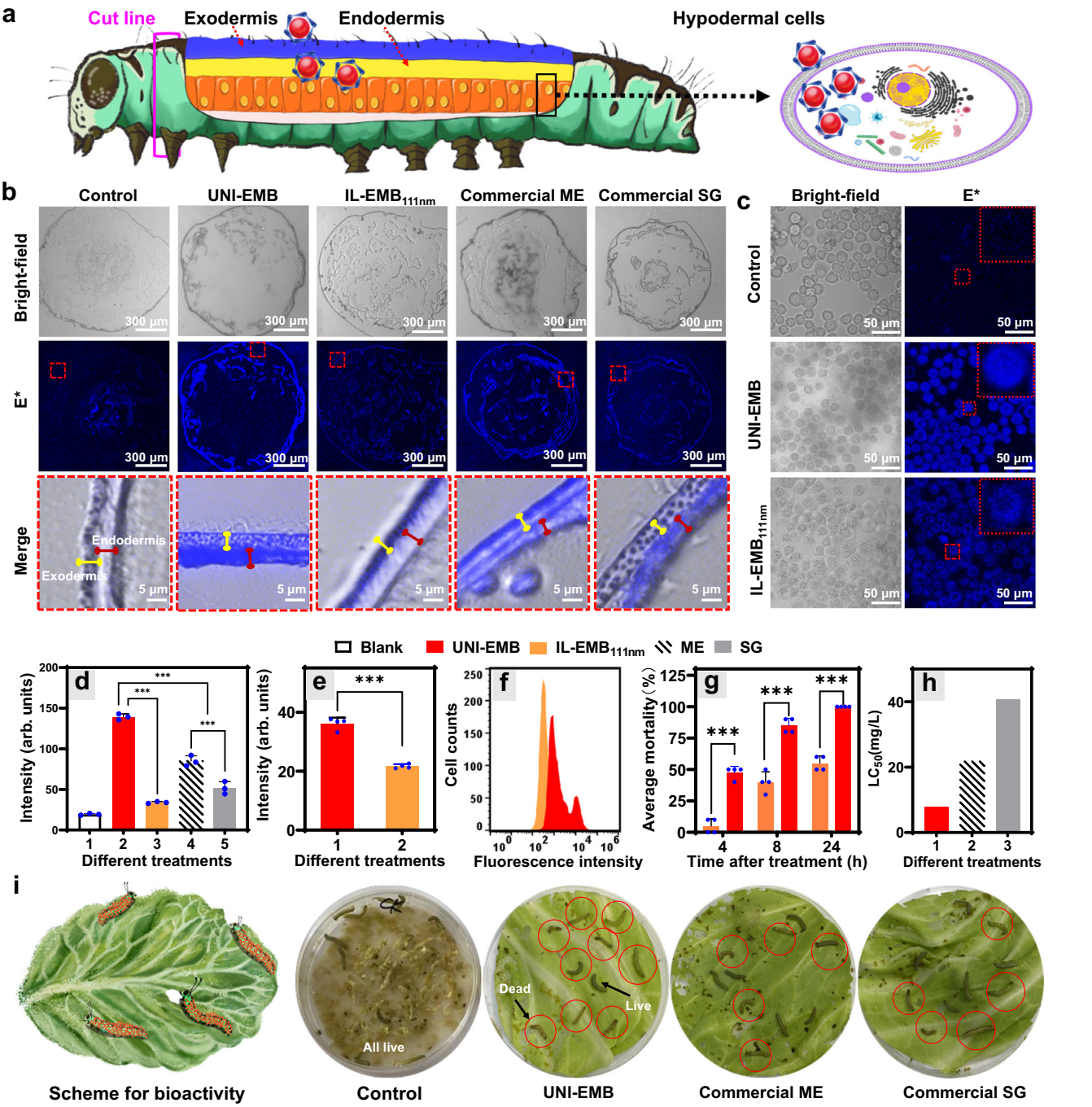

Fig. 3 | UNI-EMB performances in insect-dermis penetration, insect cellular uptake, and bioactivities. a Schematic representation of the insect-dermis and insect cell penetration process. **b** Bright-field, dark-field, and partial merge images of insect bodies with control (H_2O), UNI-EMB, IL-EMB_{111nm}, commercial microemulsion (ME), and soluble granule (SG) treatment. The red dashed box indicates the merged region. The experiments were independently repeated three times with similar results. **c** Cellular delivery/association was studied in High Five cells using confocal laser scanning microscopy (CLSM). The red dashed box delineates the magnified area. The experiments were independently repeated four times with similar results. **d** Fluorescence intensity within the endodermis (mean ± SD; $n = 3$ biological independent experiment, blank used as control). **e** Quantitative CLSM florescence intensity data of E* incubated with Hive Five cells (mean ± SD; $n = 4$ biological independent replicates, IL-EMB_{111nm} used as control). **f** Intracellular fluorescence of Hive Five cell analyzed by flow cytometry. **g** Insects were treated with EMB/CDS at concentrations of 100 mg L^{-1}, Mortality rates are shown for insects at 4 h, 8 h, and 24 h after treatment (mean ± SD; $n = 4$ biological independent replicates). **h** Median lethal concentration (LC_{50}) values were calculated from *Spodoptera exigua* larvae treated with the dipping method. **i** Visualization of larvae and leaf damage at 48 h after dipping treatment with the control (H_2O), UNI-EMB, commercial ME, or commercial WG at 62.5 mg·L^{-1}; Dead larvae are indicated by red circles. Statistical significance is calculated by one-way ANOVA with post hoc Tukey's HSD test (two-sided; multiplicity-adjusted *P* values; **d**) or two-tailed t-test (**e**, **g**).

pesticides. Our UNI demonstrated a faster release rate compared with IL-EMB_{111nm}, allowing for quicker onset of efficacy (Supplementary Fig. 17a). Further pesticide diffusion experiments showed that our UNI also has a faster diffusion rate and a higher cumulative diffusion amount (Supplementary Fig. 17b). Notably, when targeting plant cell wall barriers (<20 nm) and leaf stomata (~10 μm), our UNI can overcome these barriers to achieve effective pesticide diffusion (Supplementary Fig. 15c)[62,63]. Meanwhile, for target insects in field applications,

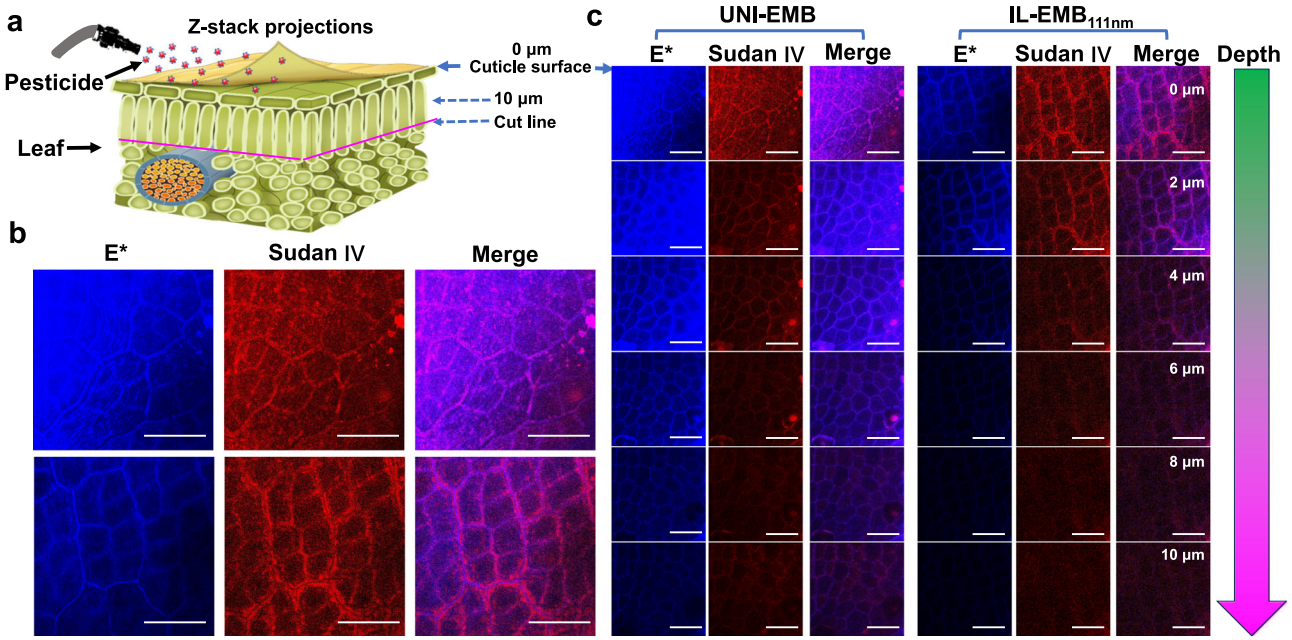

Fig. 4 | UNI-EMB performances in leaf penetration. a Foliar spray treatment. **b** E*, Sundan IV and merge images of the adaxial (upper) surface of pear leaves. **c** Z-stake profiles illustrating pear leaves treated with IL-EMB$_{111nm}$ and UNI-EMB. The difference in Z-projection depth for each sub-image was 2 μm. Scale bars = 50 μm. The experiments were independently repeated three times with similar results.

many pesticides, including EMB, exhibit synergistic effects through both contact and stomach poisoning. As shown in Fig. 3, improving the permeability of the insect cuticle is crucial for enhancing pesticide efficacy.

Effects on plant growth and normalized relative toxicity (NRT)

To characterize the effects of UNI on plant growth, physiological and biochemical indices were measured in cabbage seedlings (Fig. 6a)[64]. In terms of plant shoot dry weight, cabbage seedlings treated with UNI-EMB showed no significant differences compared to the control (water treatment) at all tested concentrations. Moreover, our results indicate that at normal application concentrations (0–50 ppm), compared to CK, the biochemical indices of UNI-treated plant seedlings, including leaf chlorophyll content, soluble protein content, superoxide dismutase (SOD) enzyme activity, and peroxidase (POD) enzyme activity, showed no significant differences (Fig. 6b-h). Furthermore, images of cabbage, broccoli, and pear following UNI-EMB treatment in the field (3.4 g·ha^{-1}, 22.5 g·ha^{-1}, 285 mg·L^{-1}, respectively) exhibited no clear symptoms of leaf injury (Fig. 6i). Additionally, the pesticide residue experiments on cabbage seedlings indicated that, compared to commercial formulations, UNI-EMB exhibited lower residues (Supplementary Fig. 18). These data suggest that UNI-EMB does not inhibit plant growth and is evidently safe for foliar application.

To assess the environmental impact of UNI, three typical, non-target organism, zebra fish (*Danio rerio*), earthworm (*Eisenia foetida*), bee (*Apis mellifera L.*) were chosen as models[65,66]. Commercial formulations, including ME and SG served as controls. The LC_{50} or median lethal dose (LD_{50}) values of UNI-EMB for zebrafish, earthworm, bee (oral feeding), and bee (topical application) were 0.15 mg·L^{-1}, 922.41 mg·L^{-1}, 0.015 μg/bee, and 0.0044 μg/bee (Fig. 7, Supplementary Fig. 19, Supplementary Tables 3–6). On the other hand, the Index of Relative Toxicity (IRT), a dimensionless number which reflects the relative pesticide activities among tested samples, is defined as the highest value of LC_{50} over the LC_{50} of the experimental samples. In our assessment, the UNI exhibited the highest pesticide activity (5.29) over both commercial controls (ME and SG, 2.82 and 1.00, respectively). We further combined both IRT and LC_{50} to better assess the toxicity towards targeted versus non-targeted organism. We defined a term, "Normalized Relative Toxicity (NRT)", as the product of the IRT of pests and the LC_{50} of the non-target organism. The NRT carries the same dimension as the LC_{50} and is expressed as:

$$NRT = IRT \times LC_{50}(\text{or}LD_{50}) \quad (1)$$

Clearly, the higher the NRT value, the higher the safety. The NRTs of UNI-EMB for zebrafish, earthworm, bee (oral feeding), and bee (topical application) were determined to be 0.79 mg·L^{-1}, 4879.55 mg·L^{-1}, 0.083 μg/bee, and 0.023 μg/bee, which were higher than all the commercial controls. The results indicate UNI-EMB has significantly higher safety compared to commercial controls.

To showcase that our UNI is an efficient delivery platform for a wide range of pesticides, we employed an environmentally friendly broad-spectrum pesticide, spinosad (SPS), to formulate UNI-SPS. Similar to UNI-EMB, UNI-SPS achieved a unimolecular state and exhibited high bioactivity against multiple pests (Supplementary Fig. 20, Supplementary Tables 7, 8)[67,68].

Discussion

We have developed a facile-fabricated, water-based, and high-efficiency unimolecular-nanopesticide(UNI)-based delivery system that results in NPs in a 3 nm-sized unimolecular state. Moreover, it is low-cost, suitable for large-scale agricultural industrialization, and field-wide application. We demonstrate that the UNI significantly enhances cellular uptake, insect-dermis translocation, and leaf-cuticle penetration of the pesticide. Our UNI system was also applied in field experiments, achieving higher control efficacy against multiple pests than two widely used commercial controls. Additionally, the low-cost raw materials used in preparing the UNI system are generally regarded as safe (GRAS) by US FDA[69]. Safety assessment on non-target organisms and plants suggests that UNI is safer than commercial controls. We are aware that a systematic assessment on UNI safety requires a third party conducting a complete study and survey[70–72]. Furthermore, our UNIs maintain very high stability during long-term storage as

https://doi.org/10.1038/s41467-025-61969-7

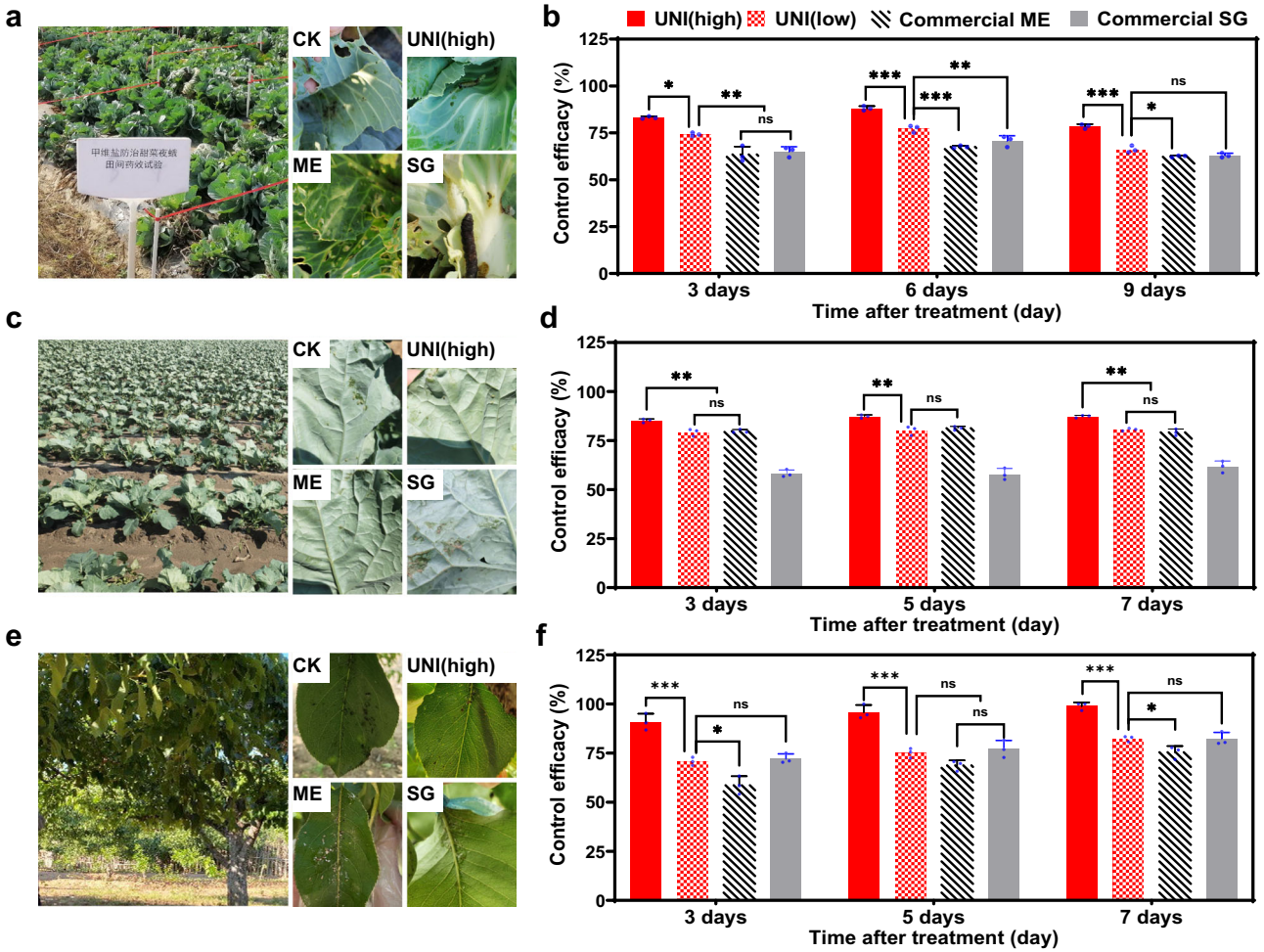

Fig. 5 | Field insecticidal efficacy of the UNI-EMB compared with commercial microemulsion (ME) and soluble granules (SG). a Images of cabbage leaves treated with CK (H_2O), UNI(high), commercial ME and SG. The word in the board means "Field efficacy trial of emamectin benzoate against the *Spodoptera exigua*". **b** Field control efficacy on *Spodoptera exigua* third instar larvae with the treatments of UNI(high) (3.4 g·ha^{-1}), UNI(low) (1.9 g·ha^{-1}), ME (3.4 g·ha^{-1}), SG (3.4 g·ha^{-1}). **c** Images of cabbage leaves treated with CK (H_2O), UNI(high), ME and SG. **d** Field control efficacy on *Brevicoryne brassicae* larvae with the treatments of UNI(high) (22.5 g·ha^{-1}), UNI(low) (18.0 g·ha^{-1}), ME (22.5 g·ha^{-1}), SG (22.5 g·ha^{-1}). **e** Images of pear leaves treated with CK (H_2O), UNI(high), ME and SG. **f** Field control efficacy on *Psylla chinensis* larvae with the treatments of UNI(high) (285 mg·L^{-1}), UNI(low) (207 mg·L^{-1}), ME (285 mg·L^{-1}) and SG (285 mg·L^{-1}). **b**, **d**, **f** $n = 3$ biological independent replicates; Data is presented as mean values ± SD. Statistical significance is calculated by one-way ANOVA with post hoc Tukey's HSD test (two-sided; multiplicity-adjusted P values).

demonstrated by their negligible changes in unimolecular pesticide size and pesticide content (Supplementary Fig. 19).

Applications of ionic liquids in pesticides have advanced tremendously partially due to the impressive success of herbicide ionic liquid (HIL)[28–41]. Our UNI system is a water-based formulation consisting of ionic liquids and active ingredients. A striking difference is that the ionic liquid in our UNI system is not the active substances, but rather the delivery system. Consequently, our UNI system has more than two types of ions. Uniquely, our UNI system is a unimolecular system with a 3 nm size that has not been reported in any other pesticide delivery systems. In the future, ionic liquids may be poised to replace traditional harmful adjuvants in insecticides, offering more environmentally friendly solutions while maintaining effective pest control. This shift signals a move towards safer and more sustainable practices in the pesticide industry, providing agricultural production with greener protective measures[73,74].

For the interaction of UNI components, the strong spatial interactions, such as electrostatic, hydrogen bonds, and van der Waals forces, among the pesticide and carriers contribute to the formulation of UNI. Further exploration of the mechanisms can be carried out using the following methods: (1) Fluorescence quenching and Förster Resonance Energy Transfer (FRET) can be used for in situ detection of molecular distances within aggregates. (2) Using single-walled carbon nanotube tips to make probes in situ, the mechanical properties of the collective and the size of the particles are used[73].

The efficiency of pesticides in the field is influenced by multiple factors during several processes, including the pesticide droplet impact, spreading, release, diffusion, and ultimately reaching the target pests. The UNI system performs efficiently in all these stages, especially in leaf penetration, cellular uptake, and insect cuticle penetration. This may be attributed to the UNI's unimolecular size, its good impact performance and spreading behavior on leaves, and more importantly, its ability to achieve rapid release and diffusion through barriers such as the epidermis and cell walls.

Our water-based UNI, made from GRAS materials, does not contain harmful organic solvents and additives such as toluene, xylene, nonylphenol, and its ethoxylates, making it safer for plants and non-target organisms. UNI has less impact on crop growth, particularly by significantly reducing pesticide residues on leaves and minimizing the health risks pesticides pose to humans. Notably, we should comprehensively evaluate the efficacy and safety of nano-pesticides, as the

https://doi.org/10.1038/s41467-025-61969-7

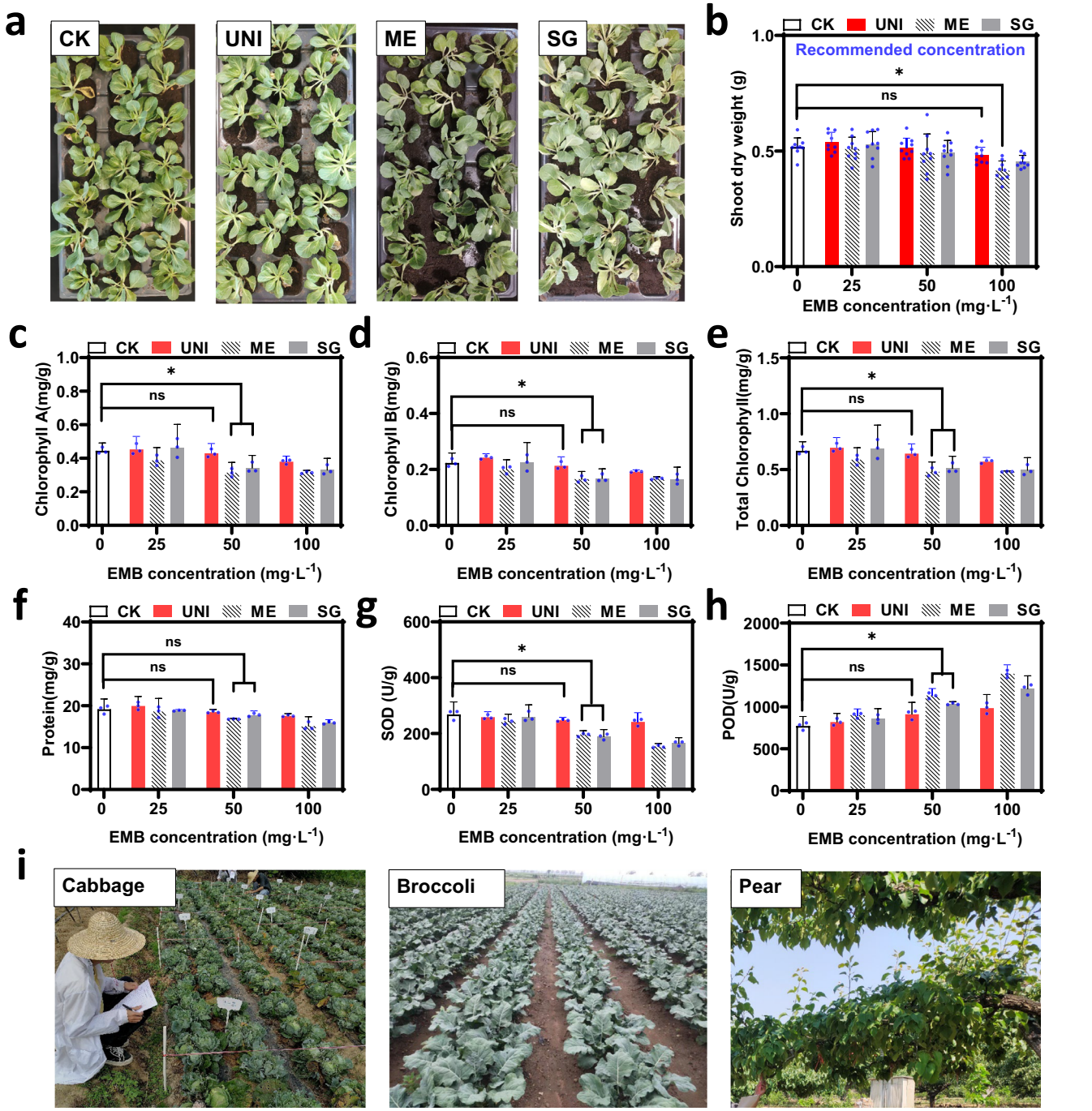

Fig. 6 | Effects on plant. a Images of cabbage seedings at 7 days treatment. The effects on shoot dry weight (**b**). chlorophyll A (**c**), chlorophyll B (**d**), total chlorophyll (**e**), protein content (**f**), SOD (**g**) and (**h**) of cabbage seedlings. **i** Images of cabbage (at 9d), broccoli (at 7 days), and pear (at 7 days) after UNI treatment (3.4 g·ha^{-1}, 22.5 g·ha^{-1}, 285 mg·L^{-1}, respectively). **b** $n = 9$ biological independent replicates; Data is presented as mean values ± SD. **c**–**h** $n = 3$ biological independent replicates; Data is presented as mean values + SD. Statistical significance is calculated by one-way ANOVA with post hoc Tukey's HSD test (two-sided; multiplicity-adjusted P values). *$p < 0.05$.

specific field application dosage is related to efficacy, which in turn determines the final dosage for non-target safety. We used the normalized relative toxicity (NRT) index to comprehensively evaluate the target pest (*Spodoptera exigua*) and non-target organisms (such as zebrafishes, bees, and earthworms), and the results showed that our UNI exhibited a higher NRT value compared to commercial formulations, indicating lower environmental risk. For field pest control on vegetable crops, our UNI significantly reduced pesticide residues compared to commercial formulations, which means higher food safety.

We explored the mechanisms underlying our UNI system through theoretical calculations and characterization experiments, including NMR, DLS, TEM, SAXS, MALDI-TOF-MS, DFT calculation, and MD simulation. These explorations revealed that the transformation of EMB from microparticles to the nano-clusters and ultimately to the unimolecular structure. In addition, our explorations highlight the importance of intermolecular interactions in facilitating water-based unimolecular systems[74,75]. This study systematically demonstrates the formation process mechanisms of the UNI system in the agricultural field.

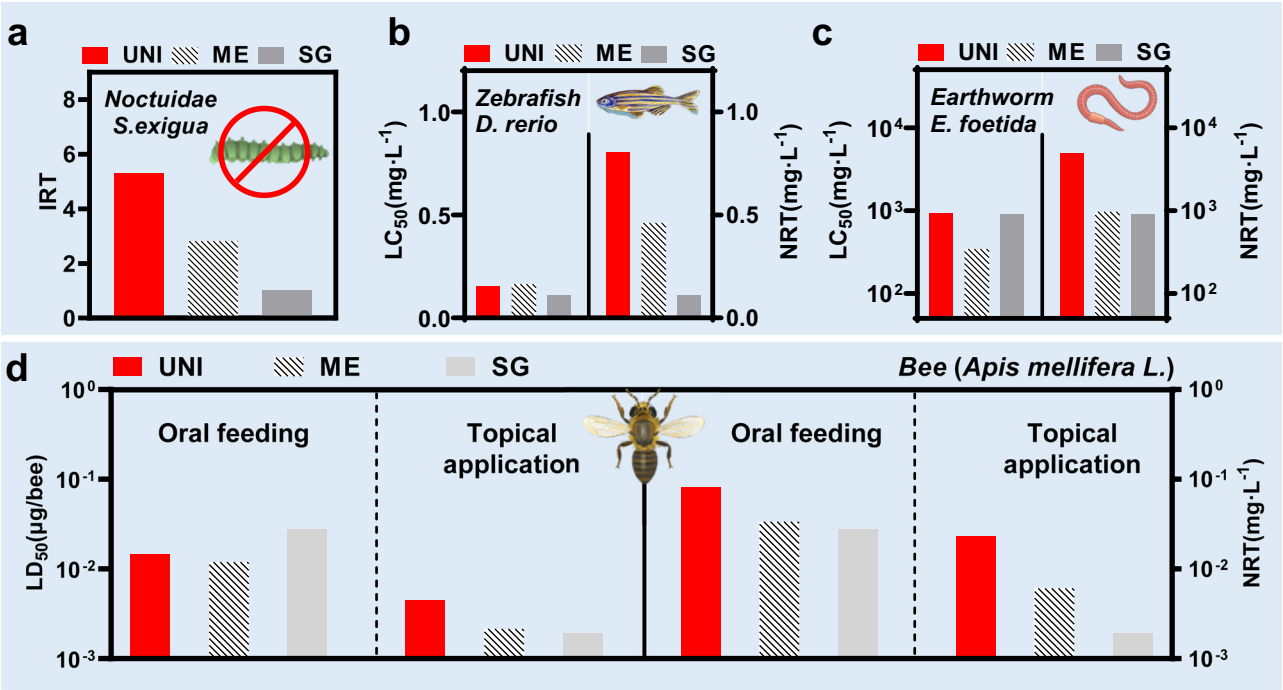

Fig. 7 | Normalized relative toxicity (NRT). a The index of the relative toxicity (IRT), which was defined as the highest value of LC_{50} over the LC_{50} of the experimental samples. **b** LC_{50} (left) and normalized relative toxicity (NRT, right) values were calculated from *D. rerio*. and IRT. NRT is defined as the product between the index of relative toxicity (IRT) of pests and the LC_{50} of non-target organism. **c** LC_{50} (left) and NRT values (right) were calculated from *E. foetida* and IRT. **d** LC_{50} (left) and NRT values (right) were calculated from *Apis mellifera L*. and IRT. "LC_{50} (left)" and "NRT (right)" refer to the values situated to the left and to the right of the solid black line in each panel.

In summary, we have developed a low-cost, water-based, and highly efficient UNI platform that enhances cellular uptake, insect-dermis, and leaf-cuticle penetration of pesticide, leading to improved field control efficacy against multiple pests. The UNI fabrication process is a one-step, simple mixture that completely avoids the use of organic solvents. Moreover, the UNI system is expected to be readily applicable for field application via plant protection drones and the system is so efficient that it can significantly reduce pesticide dosage compared with commercial ME and SG. We emphasize that our UNI system represents an efficient, multi-targeting, and safe platform that can be applied to other NPs for green pest management. Our UNI system is envisioned to play an important role in large-scale crop protection, food safety, and the development of sustainable agriculture.

Methods

Materials

High Five cells were obtained from Nanjing Agricultural University. All research complied with the relevant ethical regulations. Study protocols were approved by the Institutional Animal Care and Use Committee of Hangzhou Hunter Biotechnology, Inc. for zebrafish experiments (Protocol number IACUC-2024-9841-01).

Preparation of CDS and E*

Sodium dodecyl sulfate and choline chloride (1:1 molar ratio) were dissolved in ethanol at room temperature and stirred for 48 h. The insoluble solid was filtered and the solvent was evaporated. The product was then dried under vacuum at 50 °C for 12 h to reduce traces of ethanol and obtain choline dodecyl sulfate (CDS, Supplementary Figs. 22–25). Emamectin benzoate (EMB, 1 g, 1 mmol) and NaOH (80 mg, 2 mmol) were added to 20 mL ethanol and sonicated for 10 min, then 100 mL dichloromethane (DCM) was added. The insoluble solid was filtered, and then 185 mg (1 mmol) 1-naphthylacetic acid was added to the resulting solution. After stirring for 1 h, the solvent was evaporated, and the product was dried under vacuum at 50 °C for 12 h to obtain E* (Supplementary Figs. 25–28).

Construction of NPs

The IL-EMB_{111nm} was prepared by adding EMB and CDS (1:1 mass ratio) to a volumetric flask with water (200 mL). Subsequently, shear and high-pressure homogenization were employed to achieve uniform dispersion of IL-EMB_{111nm}. UNI-EMB and UNI-spinosad(SPS) were prepared by adding EMB/CDS (1:5 mass ratio under pH conditions adjusted to 5.3 ± 0.2 using acetic acid) and SPS/CDS (1:5 mass ratio under pH conditions adjusted to 7.0 ± 0.2 using acetic acid), respectively. Subsequently, stirred for 24 h at 25 °C. Finally, the UNI-EMB and UNI-SPS were obtained by filtration through 0.2 μm pore size membrane filters and then the pesticide concentration was adjusted to 10000 $mg{\cdot}L^{-1}$.

Characterization of the particle size and morphology

Samples were diluted with purified water. The hydrated particle size and polydispersity index (PDI) of the samples were measured using a dynamic light scattering (DLS) instrument (ZETASIZER PRO, Malvern, UK) at 25 ± 1 °C. Each sample was analyzed in triplicate, then the average values and standard deviations were calculated. The samples were also prepared for high-resolution transmission electron microscopy (HRTEM, FEI Tecnai G2 F30 S-TWIN, USA). An aliquot of resuspended aqueous NP solution was transferred onto a 300-mesh carbon-coated copper sheet to dry naturally at room temperature. Sample images were then obtained with HRTEM. Fluorescence detection was performed with a high-resolution laser confocal microscope (LSM 980, Carl Zeiss AG, Germany).

Bioactivity evaluation

Spodoptera exigua (Hübner) and *Plutella xylostella* were collected from cabbage fields in Langfang, Hebei Province, China. A laboratory colony was maintained for multiple successive generations on a standard artificial diet. Rearing conditions were set at 25 ± 5 °C, 65 ± 5% relative

humidity, under a 16 h light:8 h dark photoperiod. Third instar larvae of *Spodoptera exigua* (Hübner) and second instar larvae of *Plutella xylostella* were selected as the test insect source. Bioactivity evaluation of different EMB formulations against *Spodoptera exigua* (Hübner) third instar larvae was assayed by an indoor dipping method. The larvae were immersed for 5 s in UNI-EMB (0.32, 1.6. 8, 40, 62.5, and 100 mg·L^{-1}), commercial ME (0.64, 3.2, 16, 62.5, 80, and 125 mg·L^{-1}), and commercial SG (0.64, 3.2, 16, 62.5, 80, and 125 mg·L^{-1}), and a water treatment without EMB was used as the blank control. Larvae were dried on filter paper, then transferred to a plate, and fed fresh, untreated cabbage leaves. There were four replicates per treatment and 10 larvae per replicate. Each dish was sealed and then placed in a constant temperature incubator at 25 °C and a photoperiod of 16 h light:8 h dark. The mortality rate was examined for 48 h after treatment. Bioactivity evaluation of SPS formulations against *Plutella xylostella* second instar larvae were also evaluated using the same method. The larvae were immersed in UNI-SPS (0.0156, 0.0625, 0.25, 0.5, and 1 mg·L^{-1}), commercial EW (0.00625, 0.025, 0.1, 0.4 and 1.6 mg·L^{-1}), WG (0.02, 0.1, 0.5, 2, and 10 mg·L^{-1}) or SC (0.02, 0.1, 0.5, 2, and 10 mg·L^{-1}). The toxicity regression equation, LC_{50}, and 95% confidence interval were calculated.

Megalurothrips usitatus was collected from cowpea fields in Lincang, Yunnan, and has been reared for multiple generations on sword bean under laboratory conditions. The rearing conditions were maintained at 25 ± 5°C, 60 ± 5% relative humidity, with a 16-h light and 8-h dark photoperiod. Bioactivity evaluation of UNI-SPS against adult female *Megalurothrips usitatus* was conducted using Potter Precision Laboratory Spray Tower (Burkard). Five concentration gradients (6.25, 12.5, 25, 50, or 100 mg·L^{-1}) required for the experiment were prepared using 0.1% TritonX-100 pure water solution, with a corresponding blank control set without the pesticide. Kidney beans were cut into 4 cm pieces and placed in a plastic box measuring 6 cm in diameter and 5 cm in height. Approximately 5 mm-thick agarose was poured into the box and both sides were sealed with agarose after cooling. Each box contained around 25 adult thrips, which were immobilized using carbon dioxide before being precisely sprayed under Potter spray Tower. A volume of 2 ml of spray liquid was used each time at a pressure of 68.9 kPa, followed by settling for 30 s after each spray. The boxes were then placed at ~25 °C, about 60% relative humidity and 16 h light:8 h dark photoperiod. Their mortality status was assessed for 48 h after medication administration. Each treatment was repeated three times. The toxicity regression equation, LC_{50}, and 95% confidence interval were calculated.

Field evaluation

Field evaluation with *S. exigua* was conducted in the experimental field in Yongtang Village, Lingshan Town, Meilan District, Haikou City, Hainan Province, China (N19°59′, E110°25′). After cultivation, sections of 15 square meters in size were furrowed, and divisions were set up between sections. *S. exigua* larvae were in the third instar at the time of application. Cabbage ('Zhonggan 11') sprouts were raised on a seedbed at comparable growth stages. When the sprouts grew 4-5 leaves, they were transplanted to the field. There were three replicates for each treatment. Before treatment, the number of *S. exigua* larvae was counted. At 3, 6, and 9 days after treatment. *S. exigua* larvae were counted to calculate the control efficacy (CE) using the following equation:

$$CE(\%) = \frac{(PR - CK)}{(100 - CK)} \times 100\% \quad (2)$$

Where PR is the population decrease rate in the treatment group, and CK is the population decrease rate in the control (water) treatment group. All data from field experiments expressed as percentages were arcsine transformed to homogenize the variances before analysis.

Field evaluation with *Psylla chinensis* was conducted in the experimental field in Qianyechang Village, Anding Town, Daxing District, Beijing City, China (N39°38′, E116°33′). There were three replicates for each treatment. Before treatment, the number of *Psylla chinensis* larvae was counted. Field evaluation with *Brevicoryne brassicae* was conducted in the experimental field in Halu Village, Mantouying Town, Zhangbei County, Zhangjaikou City, Hebei Province, China (N41°14′, E114°41′). The broccoli seedlings have grown for a month. There were three replicates for each treatment. Before treatment, the number of *B. brassicae* larvae was counted. At 3, 5, and 7 days after treatment, *P. chinensis* and *B. brassicae* larvae were counted to calculate the CE.

Cabbage seedling culture

Cabbage seedlings ("Zhenlv") were cultured in organic nutrient soil. Sterilized seeds were soaked in ultra-pure water for 12 h at 30 °C, then placed in a seedling tray and covered with wet gauze. Seeds were incubated in the dark at 27 °C for 48 h to germinate. Place the germinated seeds into a seedling tray, add organic nutrient soil, and cultivate them under greenhouse conditions for 20 days. Then, the cabbage seedlings were treated with foliar spray of CK (water), UNI-EMB, commercial ME, or SG. Their EMB concentrations were 0, 25, 50, and 100 mg·L^{-1}. After 7 days of cultivation, seedlings were collected for physiological and biochemical evaluations.

Toxicity assessments in non-target organism

Adult zebrafish (*D. rerio*, AB strain) were randomly selected with an equal sex ratio and distributed in 1-L beakers with 1 L of sample in a gradient dilution. There were 10 fish in each treatment group. Water was used as the control treatment. The number of dead fish in each tank was recorded after 96 h. Fish were classified as dead if they were not breathing or did not move when the tail was touched. The mortality rate and LC_{50} were calculated by probit regression analysis. A typical method for toxicity assessments in bee (Topical application): Preparing solutions with methanol at five concentrations (such as 0.50, 1.00, 2.00, 4.00, and 8.00 mg·L^{-1}). Bees are introduced into an Erlenmeyer flask, which is sealed with gauze, and anesthetized with nitrogen gas. Using an electric pipette, 1.00 μL of the test solution at each concentration is applied to the dorsal thorax of each bee. A methanol control group (CK) is also set up. Both the treatment and control groups are conducted with 3 replicates, each containing 10 bees. Once the bees have dried, they are transferred to test cages and fed with 50% (w/w) sucrose solution. The mortality rate and LD_{50} were calculated by probit regression analysis. A typical method for toxicity assessments in bee (Oral feeding): Pesticides are diluted with a 50% (mass concentration) sucrose solution to five concentrations (such as 0.0625, 0.125, 0.250, 0.500, and 1.00 mg·L^{-1}) sucrose solutions. Bees from the storage cage are transferred to the test cage, and 200 μL of the sucrose solution containing the test substance is added to the feeder, with a blank control group set up. Both the treatment and control groups are replicated 3 times, each with 10 bees. Since the bees refused to feed, resulting in low food consumption, the feeders are removed after 6 h and replaced with pesticide-free sucrose solution for ad libitum feeding. At the same time, the consumption of each group's solution is measured by determining the weight of the remaining food. The mortality rate and LD_{50} were calculated by probit regression analysis. A typical method for toxicity assessments in earthworm: Pesticide solutions were prepared at five different concentrations (such as 500, 250, 125, 62.5, and 31.25 mg·L^{-1}). The healthy earthworms were introduced into culture dishes, and then the prepared pesticide solutions were added with 1 mL per dish. Both the treatment and control groups are conducted with 3 replicates. A water control group (CK) is also set up. The mortality rate of the earthworms for pesticide treatment was assessed after 1 day. The mortality rate and LC_{50} were calculated by probit regression analysis.

Statistical analysis
Significant differences between more than two groups were determined using a one-way analysis of variance (ANOVA) followed by a post-hoc Duncan's multiple comparisons between groups, or were determined using a two-tailed t-test for two groups.

Reporting summary
Further information on research design is available in the Nature Portfolio Reporting Summary linked to this article.

Data availability
The data generated in this study are provided in the Supplementary Information/Source Data file. Figure 1a, c and Supplementary Fig. 1c were created with MedPeer (medpeer.cn). All data underlying this study are available from the corresponding author upon request.

References

1. Kah, M. et al. A critical evaluation of nanopesticides and nanofertilizers against their conventional analogues. *Nat. Nanotechnol.* **13**, 677–684 (2018).
2. Lamberth, C. et al. Current challenges and trends in the discovery of agrochemicals. *Science* **341**, 742–746 (2013).
3. Verger, P. J. P. & Boobis, A. R. Reevaluate pesticides for food security and safety. *Science* **341**, 717–718 (2023).
4. Hough, R. L. A world view of pesticides. *Nat. Geosci.* **14**, 180–184 (2021).
5. Zhang, L. et al. Coacervate-enhanced deposition of sprayed pesticide on hydrophobic/superhydrophobic abaxial leaf surfaces. *Adv. Sci.* **10**, 2300270 (2023).
6. Gao, C. et al. A user-friendly herbicide derived from photoresponsive supramolecular vesicles. *Nat. Commun.* **9**, 2967 (2018).
7. Wang, Z. et al. Functionalized carbon dot-delivered RNA nano fungicides as superior tools to control phytophthora pathogens through plant RdRP1-mediated spray-induced gene silencing. *Adv. Funct. Mater.* **33**, 2213143 (2023).
8. Zong, M. et al. Redox and near-infrared light-responsive nanoplatform for enhanced pesticide delivery and pest control in rice: construction, efficacy, and potential mechanisms. *ACS Appl. Mater. Interfaces* **15**, 41351–41361 (2023).
9. Lowry, G. V., Avellan, A. & Gilbertson, L. M. Opportunities and challenges for nanotechnology in the agri-tech revolution. *Nat. Nanotechnol.* **14**, 712–718 (2019).
10. Kah, M., Tufenkji, N. & White, J. C. Nano-enabled strategies to enhance crop nutrition and protection. *Nat. Nanotechnol.* **14**, 532–540 (2019).
11. Zhang, P. et al. Nanotechnology and artificial intelligence to enable sustainable and precision agriculture. *Nat. Plants* **7**, 864–876 (2021).
12. Shelar, A. et al. Recent advances in nano-enabled seed treatment strategies for sustainable agriculture: challenges, risk assessment, and future perspectives. *Nano Micro Lett.* **15**, 54 (2023).
13. Liang, W. pH-responsive on-demand alkaloids release from core–shell ZnO@ZIF-8 nanosphere for synergistic control of bacterial wilt disease. *ACS Nano* **16**, 2762–2773 (2022).
14. Wang, D. et al. Nano-enabled pesticides for sustainable agriculture and global food security. *Nat. Nanotechnol.* **17**, 347–360 (2022).
15. Lowry, G. V. et al. Towards realizing nano-enabled precision delivery in plants. *Nat. Nanotechnol.* **19**, 1255–1269 (2024).
16. Du, Q. et al. Thermo-responsive liposome nano-vesicles for co-delivery of emamectin benzoate and nitenpyram with synergistic pest control. *Chem. Eng. J.* **479**, 147548 (2024).
17. Wang, J. et al. Evaluation of a spinosad controlled-release formulation based on chitosan carrier: insecticidal activity against *Plutella xylostella* (L.) larvae and dissipation behavior in soil. *ACS Omega* **6**, 30762–30768 (2021).
18. An, C. et al. Polylactic acid nanoparticles for co-delivery of dinotefuran and avermectin against pear tree pests with improved effective period and enhanced bioactivity. *Int. J. Biol. Macromol.* **206**, 633–641 (2022).
19. Zhang, L. et al. Nanodelivery system alters an insect growth regulator's action mode: from oral feeding to topical application. *ACS Appl. Mater. Interfaces* **14**, 35105–35113 (2022).
20. Tang, J. et al. Deposition and water repelling of temperature-responsive nanopesticides on leaves. *Nat. Commun.* **14**, 6401 (2023).
21. Shen, Y. et al. Temperature-dependent nanogel for pesticide smart delivery with improved foliar dispersion and bioactivity for efficient control of multiple pests. *ACS Nano* **16**, 20622–20632 (2022).
22. Leng, Y. Analysis on the development trend of pesticide formulation from market, regulations, and technology in China. *World Pestic.* **42**, 1–7 (2020).
23. Guo, Y., Liu, F., Wang, J. & Peng, Q. Research progress on the substitution of harmful organic solvents in pesticide emulsifiable concentrates. *Chin. J. Pestic. Sci.* **22**, 925–932 (2020).
24. Knowles et al. Recent developments of safer formulations of agrochemicals. *Environmentalist* **28**, 35–44 (2008).
25. Feng J. et al. Application of nanoemulsions in formulation of pesticides. in *Nanoemulsions* (eds Jafari, S.M. & McClements, D. J.) 379–413 (Academic Press, 2018).
26. Tian, Y. et al. A simple preparation process for an efficient nanoformulation: small molecule self-assembly based on spinosad and sulfamic acid. *Green. Chem.* **23**, 4882–4891 (2021).
27. An, C. et al. Design and synthesis of a water-based nanodelivery pesticide system for improved efficacy and safety. *ACS Nano* **18**, 662–679 (2024).
28. Pernak, J., Syguda, A., Janiszewska, D., Materna, K. & Praczyk, T. Ionic liquids with herbicidal anions. *Tetrahedron* **67**, 4838–4844 (2011).
29. Pernak, J. et al. Bioinspired herbicides–ionic liquids or liquid cocrystals? *J. Agric. Food Chem.* **72**, 1454–1461 (2024).
30. Pernak, J. et al. Dicationic herbicidal ionic liquids comprising two active ingredients exhibiting different modes of action. *J. Agric. Food Chem.* **70**, 2545–2553 (2020).
31. Pernak, J. et al. Dicamba-based herbicides: Herbicidal ionic liquids versus commercial forms. *J. Agric. Food Chem.* **68**, 4588–4594 (2020).
32. Szymaniak, D. et al. Synthesis and characterization of double-salt herbicidal ionic liquids comprising both 4-chloro-2-methylphenoxyacetate and trans-cinnamate anions. *ChemPlusChem* **85**, 2281–2289 (2020).
33. Wilms, W. et al. Herbicidal ionic liquids: a promising future for old herbicides? Review on synthesis, toxicity, biodegradation, and efficacy studies. *J. Agric. Food Chem.* **68**, 10456–10488 (2020).
34. Czuryszkiewicz, D. et al. Herbicidal ionic liquids containing the acetylcholine cation. *ChemPlusChem* **84**, 268–276 (2019).
35. Marcinkowska, K. et al. Herbicidal ionic liquids containing double or triple anions as a new potential tool for weed control including herbicide-resistant biotypes. *Crop Prot.* **169**, 106238 (2023).
36. Parus, A. et al. Evaluation of the influence of different cations on the mobility and performance of dicamba-based ionic liquids. *J. Environ. Chem. Eng.* **10**, 108397 (2022).
37. Wilms, W. et al. Glyphosate versus glyphosate-based ionic liquids: Effect of cation on glyphosate biodegradation, soxA and phnJ genes abundance and microbial populations changes during soil bioaugmentation. *Chemosphere* **316**, 137717 (2023).
38. Parus, A. et al. Can ionic liquids exist in the soil environment? Effect of quaternary ammonium cations on glyphosate sorption, mobility and toxicity in the selected herbicidal ionic liquids. *J. Mol. Liq.* **334**, 116452 (2023).

39. Lisiecka, N. et al. Unraveling the effects of acrylonitrile butadiene styrene (ABS) microplastic ageing on the sorption and toxicity of ionic liquids with 2,4-D and glyphosate herbicides. *Chemosphere* **364**, 143271 (2024).
40. Piotrowska, A. et al. Effects of ammonium-based ionic liquids and 2, 4-dichlorophenol on the phospholipid fatty acid composition of zebrafish embryos. *PLoS ONE* **13**, e0190779 (2018).
41. Homo, J. et al. Ecotoxicity studies reveal that organic cations in dicamba-derived ionic liquids can pose a greater environmental risk than the herbicide itself. *Sci. Total Environ.* **922**, 171062 (2024).
42. Lewis C. T. The penetration of cuticle by insecticides. In *Cuticle Techniques in Arthropods* (ed Miller T.) 367–400 (Springer, 1980).
43. Jain, R. G. et al. Foliar application of clay-delivered RNA interference for whitefly control. *Nat. Plants* **8**, 535–548 (2022).
44. Avellan, A. et al. Nanoparticle size and coating chemistry control foliar uptake pathways, translocation, and leaf-to-rhizosphere transport in wheat. *ACS Nano* **13**, 5291–5305 (2019).
45. Rana, A. S. et al. Microemulsions as potential pesticidal carriers: a review. *J. Mol. Liq.* **390**, 122969 (2023).
46. Tanner, E. E. L. et al. Design principles of ionic liquids for transdermal drug delivery. *Adv. Mater.* **31**, 1901103 (2019).
47. Radlinski, A. P. et al. Application of SAXS and SANS in evaluation of porosity, pore size distribution and surface area of coal. *Int J. Coal Geol.* **59**, 245–271 (2004).
48. Pracht, P., Bohle, F. & Grimme, S. Automated exploration of the low-energy chemical space with fast quantum chemical methods. *Phys. Chem. Chem. Phys.* **22**, 7169–7192 (2020).
49. Grimme, S., Bannwarth, C. & Shushkov, P. A robust and accurate tight-binding quantum chemical method for structures, vibrational frequencies, and noncovalent interactions of large molecular systems parametrized for all spd-block elements (Z=1–86). *J. Chem. Theory Comput.* **13**, 1989–2009 (2017).
50. Gaussian 16, Revision A.03.
51. Lee, C., Yang, W. & Parr, R. G. Development of the colle-salvetti correlation-energy formula into a functional of the electron density. *Phys. Rev. B.* **37**, 785–789 (1988).
52. Lu, T. & Chen, F. W. Multiwfn: a multifunctional wavefunction analyzer. *J. Comput. Chem.* **33**, 580–592 (2012).
53. Lu, T. & Chen, Q. X. Independent gradient model based on Hirshfeld partition: a new method for visual study of interactions in chemical systems. *J. Comput. Chem.* **43**, 539–555 (2022).
54. Emamian, S., Lu, T., Kruse, H. & Emamian, H. Exploring nature and predicting strength of hydrogen bonds: a correlation analysis between atoms-in-molecules descriptors, binding energies, and energy components of symmetry-adapted perturbation theory. *J. Comput. Chem.* **40**, 2868–2881 (2019).
55. Robertson, M. J., Tirado-Rives, J. & Jorgensen, W. L. Improved peptide and protein torsional energetics with the OPLS-AA force field. *J. Chem. Theory Comput.* **11**, 3499–3509 (2015).
56. Abraham, M. J., Murtola, T., Schulz, R., Páll, S. & Lindahl, E. GROMACS: high performance molecular simulations through multi-level parallelism from laptops to supercomputers. *SoftwareX* **1-2**, 19–25 (2015).
57. Humphrey, W., Dalke, A. & Schulten, K. VMD: visual molecular dynamics. *J. Mol. Graph.* **14**, 33–38 (1996).
58. Hockney, R. W., Goel, S. P. & Eastwood, J. W. Quiet high-resolution computer models of a plasma. *J. Comput. Phys.* **14**, 148–158 (1974).
59. Shi, Y. et al. Divergent amplifications of CYP9A cytochrome P450 genes provide two noctuid pests with differential protection against xenobiotics. *Proc. Natl Acad. Sci. USA* **120**, e2308685120 (2023).
60. Dong, Y. et al. Control of a sap-sucking insect pest by plastid-mediated RNA interference. *Mol. Plant* **15**, 1176–1191 (2022).
61. Ma, Y. et al. A pH/cellulase dual stimuli-responsive cellulose-coated metal–organic framework for eco-friendly fungicide delivery. *Chem. Eng. J.* **462**, 142190 (2023).
62. Demirer, G. S. et al. High aspect ratio nanomaterials enable delivery of functional genetic material without DNA integration in mature plants. *Nat. Nanotechnol.* **14**, 456–464 (2019).
63. Kurepa, J. et al. Uptake and distribution of ultrasmall anatase TiO_2 alizarin red S nanoconjugates in *Arabidopsis thaliana*. *Nano Lett.* **10**, 2296–2302 (2010).
64. Guo, H. et al. Salivary carbonic anhydrase II in winged aphid morph facilitates plant infection by viruses. *Proc. Natl Acad. Sci. USA* **120**, e2222040120 (2023).
65. Zhang, D.-x et al. Core/shell dual-responsive nanocarriers via iron-mineralized electrostatic self-assembly for precise pesticide delivery. *Adv. Funct. Mater.* **31**, 2102027 (2021).
66. Luo, J. et al. Self-assembled degradable nanogels provide foliar affinity and pinning for pesticide delivery by flexibility and adhesiveness adjustment. *ACS Nano* **15**, 14598–14609 (2021).
67. Guo, Z. et al. Retrotransposon-mediated evolutionary rewiring of a pathogen response orchestrates a resistance phenotype in an insect host. *Proc. Natl Acad. Sci. USA* **120**, e2300439120 (2023).
68. Wu, M. et al. Efficient control of western flower thrips by plastid-mediated RNA interference. *Proc. Natl Acad. Sci. USA* **120**, e2120081119 (2022).
69. Su, Y. et al. Cost–benefit analysis of nanofertilizers and nanopesticides emphasizes the need to improve the efficiency of nanoformulations for widescale adoption. *Nat. Food* **3**, 1020–1030 (2022).
70. Hofmann, T. et al. Technology readiness and overcoming barriers to sustainably implement nanotechnology-enabled plant agriculture. *Nat. Food* **1**, 416–425 (2020).
71. Kah, M. et al. Comprehensive framework for human health risk assessment of nanopesticides. *Nat. Nanotechnol.* **16**, 955–964 (2021).
72. Shangguan, W. et al. Nano-micro core–shell fibers for efficient pest trapping. *Nano Lett.* **23**, 11809–11817 (2023).
73. Li, Y. et al. Controlled assembly of dendrimer-like DNA. *Nat. Mater.* **3**, 38–42 (2004).
74. Bao, Z. et al. Molecular selection and environmental evaluation of eco-friendly surfactants to efficiently reduce pesticide pollution. *J. Clean. Prod.* **416**, 137954 (2023).
75. Wang, Y. et al. High-efficiency green management of potato late blight by a self-assembled multicomponent nano-bioprotectant. *Nat. Commun.* **14**, 5622 (2023).

Acknowledgements

We are grateful for financial support from the National Key R&D Program of China (2021YFA0716704, 2022YFD1401200) to Y.W., the National Natural Science Foundation of China (No. 22308375 to X. Li. and No. 22478416 to Y. W.) and the Agricultural Science and Technology Innovation Program (CAAS-BRC-GLCA-2025-01 to Y.W., CAAS-CSCB-202402 to X.L., CAAS-CSGLCA-IEDA-202401 to Y.W., and BSRF202510 to Y.S.). We appreciate the kind help of Prof. Shuwen Wu and Prof. Yu Shi from Nanjing Agricultural University, as well as Prof. Peifeng Liu from Shanghai Jiao Tong University. We thank the staff at the BL19U2 beamline of the NFPS at Shanghai Synchrotron Radiation Facility for assistance with data collection.

Author contributions

X.L. and Y.W. conceived the idea and designed the experiments; X.L. performed most of the experiments. X.L., X.W., C.S., and A.W. developed the methodology and analyzed the data; N.L., Y.S., J.H., H.L., and J. X. assisted in collecting the data. X.L. and Y.W. wrote the manuscript. D.L. and Y.W. provided comments and edited the manuscript.

Competing interests

The authors declare no competing interests.

Additional information

Supplementary information The online version contains supplementary material available at https://doi.org/10.1038/s41467-025-61969-7.

Correspondence and requests for materials should be addressed to Yan Wang.

Peer review information *Nature Communications* thanks the anonymous reviewers for their contribution to the peer review of this work. A peer review file is available.